

Skarn Formation in Metamorphic Rocks of the Chungju Mine Area

Gun-Soo Kim* and Maeng-Eon Park*

ABSTRACT: Tungsten skarns in the Chungju mine which consists mainly of strata-bound type iron ore deposits are found in the vicinity of the contact between the age-unknown Kyemeongsan Formation and granitic rock intrusions of Mesozoic age (134 ± 2 Ma). Tungsten skarns were formed extensively from alumina and silica-rich schistose rocks by the introduction of calcium and iron from hydrothermal solution. The skarns comprise a metasomatic column and are subdivided into four facies; garnet facies, wollastonite facies, epidote facies and chlorite facies. The skarn process in time-evolutional trend can be divided broadly into the four facies in terms of the paragenetic sequence of calc-silicates and their chemical composition. Skarn and ore minerals were formed in the following sequence; (1) garnet facies, adjacent to biotite granite, containing mainly garnet (>Ad96) and magnetite, (2) wollastonite facies containing mainly wollastonite and garnet (Ad95~60), (3) epidote facies, containing mainly epidote (Ps35~31), quartz, andradite-grossular (Ad63~50), and scheelite, (4) chlorite facies, adjacent to and replacing schist, containing mainly chlorite, muscovite, quartz, calcite, epidote (Ps31~25), hematite and sulfides. The mineral assemblage and mineral compositions suggest that the chemical potentials of Ca and Fe increased toward the granitic rock, and the component Al, Mg, K, and Si decreased from the host rock to granitic rock. The homogenization temperature and salinity of fluid inclusion in scheelite, quartz and epidote of epidote facies skarn is $300 \sim 400^\circ\text{C}$ and 3~8wt.% equiv. NaCl, respectively. $\delta^{34}\text{S}$ values of pyrite and galena associated with chlorite facies skarn is 9.13~9.51‰ and 5.85~5.96‰, respectively. The temperature obtained from isotopic composition of coexisting pyrite-galena is $283 \pm 20^\circ\text{C}$. Mineral assemblages and fluid inclusion data indicate that skarn formed at low X_{CO_2} , approximately 0.01. Temperature of the skarn mineralization are estimated to be in the range of 400°C to 260°C and pressure to be 0.5 kbar. The oxygen fugacity (f_{O_2}) of the skarn mineralization decreased with time. The early skarn facies would have formed at log f_{O_2} values of about -25 to -27, and late skarn facies would have formed at log f_{O_2} values of -28 to -30. The estimated physicochemical condition during skarn formation suggests that the principal causes of scheelite mineralization are reduction of the ore-forming fluid and a decrease in temperature.

INTRODUCTION

The Chungju mine is located about 5km southwest of the Chungju City (Fig. 1). Iron ore deposits in Chungju mining area is well known as the strata-bound type in Korea (Kim, 1977; Lee, 1980; Kim, 1991). Iron ore bodies occur as layers and lens-shaped bodies in the metamorphic rocks which were intruded by Mesozoic granitic rocks. The metamorphic rocks of the Chungju mining area are known as Kyemeongsan Formation and composed of schistose rocks and iron-bearing quartzite.

Tungsten skarn occurs in the contact of schistose rocks and granitic rocks. Although the skarn mineralization is developed in small scale and not sufficient resources potential, it is particular interest related to iron ore genesis. Many investigators (Kim and Lee, 1965; Lee, 1977; Reedman *et al.*, 1973; Cruzel, 1991) have studied the geology and ore geneses of iron ore, but little is known

about the skarnization which associated with tungsten mineralization.

This paper presents the geology, mineralogy, and geochemistry of tungsten-bearing skarn. We also describe the history of skarn formation in the Chungju district, paying particular attention to the accompanying mineralogic and chemical changes in silicate gangue. Research in this study involved field mapping, petrographic examination and the electron microprobe analysis of selected samples. Fluid inclusion and stable isotopic study were performed on the samples from skarn zone.

GEOLOGY

The mine area consists of metamorphic rocks (Kyemeongsan Formation) and igneous rocks (Fig. 1). The metamorphic rocks are mainly composed of schistose rocks and iron-bearing quartzite. The schistose rocks, the dominant rock type of the area, are foliated and/or finely banded by the presence of platy minerals. The

*Department of Applied Geology, College of Marine Science and Technology, National Fisheries University of Pusan, Pusan 608-737, Korea

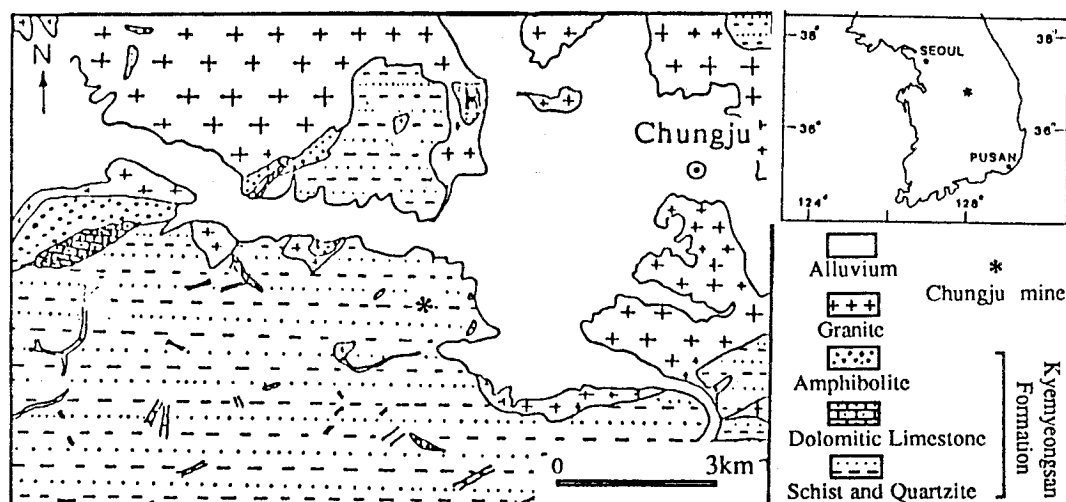


Fig. 1. Geological map of the Chungju mining district (modified after by Kim and Lee, 1965).

Table 1. Rb-Sr isotopic data for the biotite granite from Chungju mine.

Sample no.	Rb-Sr data : whole rock isochron				Isochron parameters			
	Rb (ppm)	Sr (ppm)	$^{87}\text{Sr}/^{86}\text{Sr}$	$\pm 2\sigma$	$^{87}\text{Rb}/^{86}\text{Sr}$	Slope ($\times 10^{-3}$)	Intercept	Data (Ma $\pm 1\sigma$)
CJ-817	43.9	555.9	0.7132744	10	0.228619	1.9109	0.71314	134 \pm 2.0
CJ-712	162.4	452.8	0.7154019	9	1.038456			
CJ-784	160.3	421.2	0.7152353	8	1.101914			
CJ-307	175.7	434.3	0.7154228	12	1.171363			
CJ-710	276.8	76.2	0.7332783	8	10.554518			

rocks can be subdivided into quartz schist, quartz-mica schist and quartz-feldspar schist. As the feature of the schistose rocks changes gradationally, it is very difficult to define their lithologic boundaries. Iron-bearing quartzite, the dominant iron ores of the region, is commonly intercalated with schistose rocks. The iron-bearing quartzite shows a relatively distinct contact with schistose rocks. The metamorphic grade of Chungju mine area is reported as lower amphibolite facies by Lee(1980). Generally, trend of foliation shows a strike of $N50^{\circ} \sim 70^{\circ}E$, and a dip of $60^{\circ} \sim 80^{\circ}SE$, though it is highly variable in places. Igneous rocks, known as the Chungju granite(Kim and Lee, 1965), are widely exposed in mine area. The granitic rocks composed of biotite granite and hornblende granite. The biotite granite which regionally occur as stocks cut across the metamorphic rocks. Hornblende granite occur as small stock, and intruded by the biotite granite.

The biotite granite which are considered to skarn related intrusion cut across the metamorphic rocks. The biotite granite is composed of quartz(31.1%), potassium feldspar(27.4%), plagioclase (24.9%), biotite(7.6%), with minor amount of hornblende, epidote, chlorite and

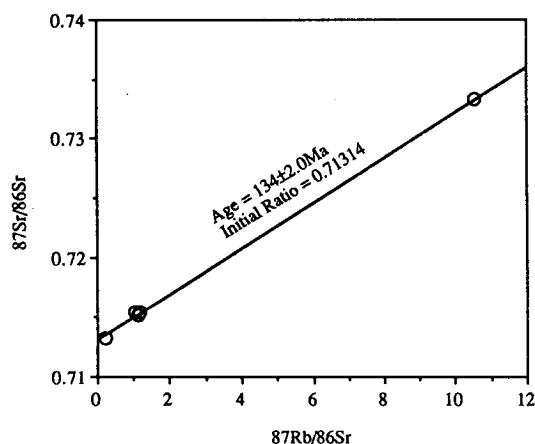


Fig. 2. Rb-Sr whole rock isochron diagram for the biotite granite in Chungju mine.

sphe. Modal content of quartz, plagioclase and biotite tend to decrease in the granite at the contact with skarn body but potassium feldspar, chlorite and magnetite increase. Mafic minerals are altered to chlorite, and feldspars are altered to epidote or sericite near the skarn

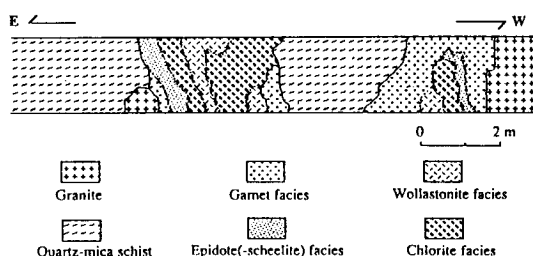


Fig. 3. Schematic distribution of skarn facies near biotite granite and quartz-mica schist contact in the Chungju mine (at -2 level, the main ore body).

zone. A Rb-Sr isochron age of the biotite granite is 134 ± 2 Ma (Table 1, Fig. 2). The quartz-mica schist which is invaded rock of skarn is composed of quartz, biotite, potassium feldspar, plagioclase, epidote, chlorite and calcite. It is characterized by granoblastic texture. Fine- to medium-grained polygonal quartz and lath-shaped

plagioclase are tightly interlocked. Platy aggregates of biotite often define foliated structure of the rock.

Dolomitic limestone occurs in the northwestern part of Chungju mine, but any block of limestone is not found in the mine area.

DESCRIPTION OF SKARNS

Skarns are developed in small scale at the contact between the biotite granite and quartz-mica schist. Typical and fairly amounts of skarn occurs at the Central Drift and lower 2nd level (Kim, 1991). Some skarns have been observed in direct contact with biotite granite but some other skarns are isolately formed in quartz-mica schist without contact to the biotite granite. Although the skarn being considered here are mineralogically heterogeneous, there are some consistent zonal patterns in distribution. Granite is highly altered at its margin contacting with skarn zone but the altered margin did

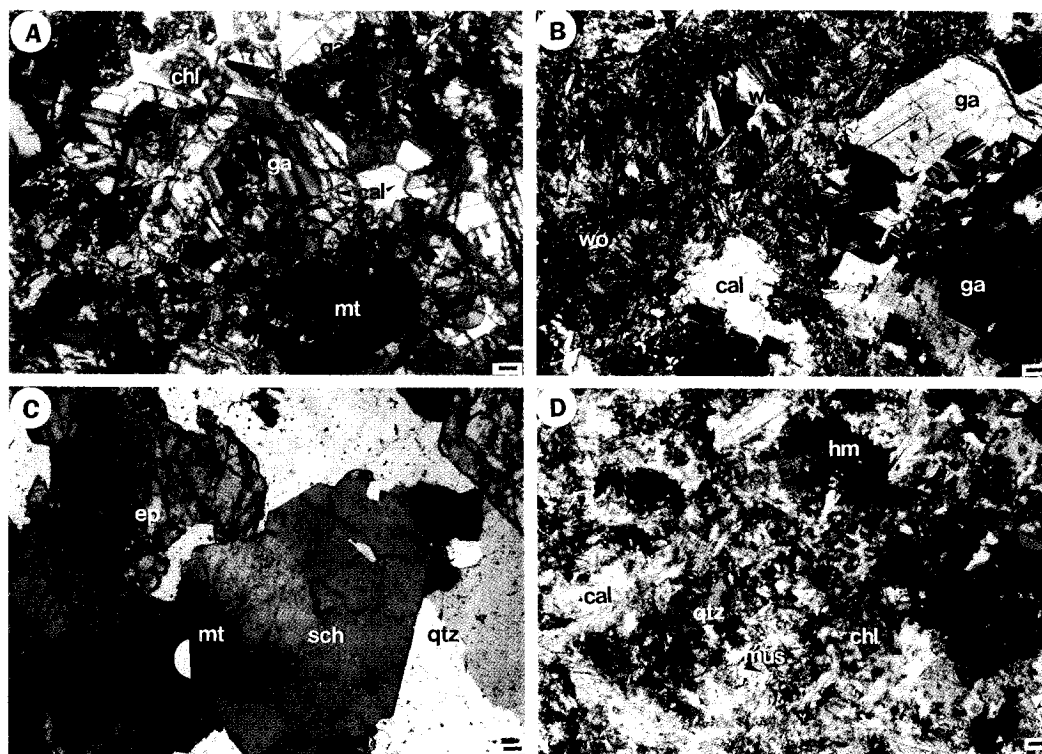


Fig. 4. Photomicrographs showing the mode of occurrence of skarn minerals from skarn facies. A; Zoned anisotropic garnet (ga) in garnet facies replaced by calcite (cc) veinlet and are filled with late chlorite (chl) and calcite. Magnetite is contained in garnet grains. B; Wollastonite (wo) is partly replaced to garnet in wollastonite facies. Two types of garnet are recognized. C; Scheelites (sch) in epidote facies coexisting with epidote (ep) and quartz (qtz). D; Chlorite occurs as radiating aggregates or discrete grains in chlorite facies. Fan-shaped muscovite (mus) and anhedral quartz occur between interstices and inside of calcite. Scale bars indicate 0.1 mm.

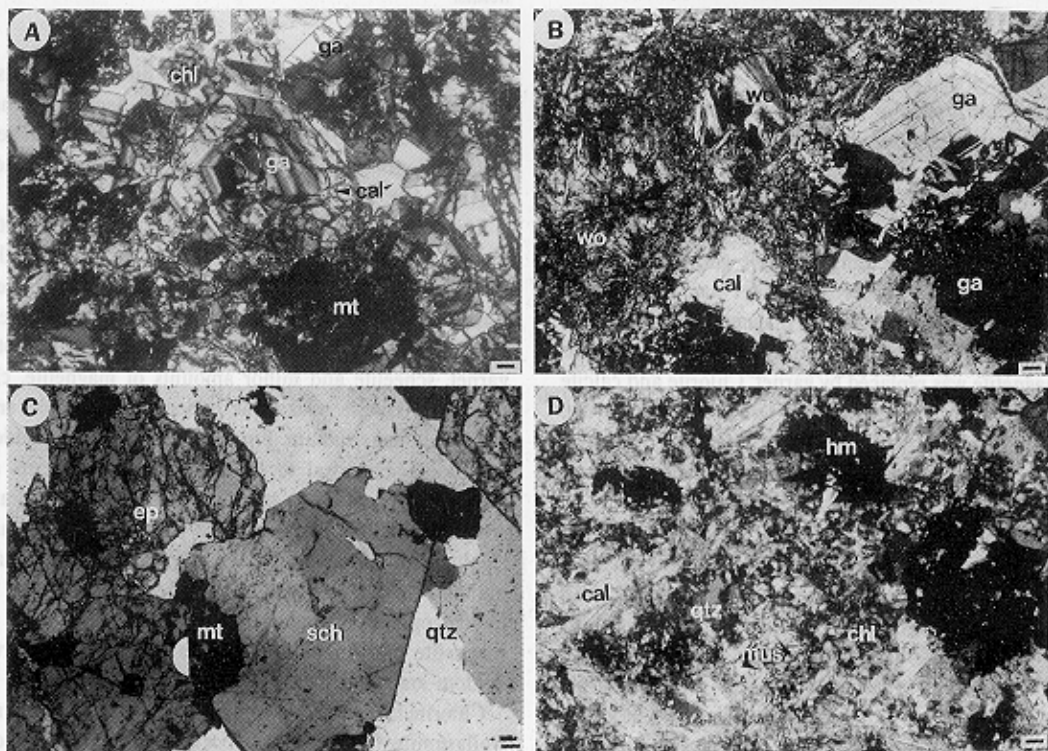


Fig. 4. Photomicrographs showing the mode of occurrence of skarn minerals from skarn facies. A; Zoned anisotropic garnet(ga) in garnet facies replaced by calcite(cc) veinlet and are filled with late chlorite(chl) and calcite. Magnetite is contained in garnet grains. B; Wollastonite(wo) is partly replaced to garnet in wollastonite facies. Two types of garnet are recognized. C; Scheelites(sch) in epidote facies coexisting with epidote(ep) and quartz(qtz). D; Chlorite occurs as radiating aggregates or discrete grains in chlorite facies. Fan-shaped muscovite(mus) and anhedral quartz occur between interstices and inside of calcite. Scale bars indicate 0.1 mm.

not form any skarnization.

The metasomatic process of skarn growth in the time-evolutional trend can be divided broadly into the four skarn facies in terms of the paragenetic sequence of calc-silicates and their chemical composition. Based on the mineral assemblage, the skarn can be classified into garnet facies, wollastonite facies, epidote-(scheelite) facies and chlorite facies (Fig. 3). The skarn facies is generally gradual, but in some places it is obvious.

The spatial distribution of these skarn facies, their mineralogy, and the chemical composition of the mineral particularly which occur in more than one skarn facies, indicate that the skarn facies comprise a chemically and spatially related. The spatial distribution of skarn facies at Chungju mine area shows a general sequence of garnet facies, wollastonite facies, epidote facies and chlorite facies from the intrusion contact.

Garnet facies is developed on the biotite granite side of skarn. It is a few meter to a few centimeter in width and contact the biotite granite with a sharp contact. Garnet and magnetite are major constituent, and small amount of calcite, chlorite, hematite and pyrite are associated. Garnet is more coarser grained (1 to 3 mm) than other associated minerals and euhedral to subhedral in shape (Fig. 4A). The garnet is generally reddish brown in color and optically isotropic to weakly anisotropic. Larger grains generally exhibit slightly optical zoning which parallels crystal faces. Optically isotropic garnet has a composition close to pure andradite. However, a small amount of optically anisotropic garnet is observed and occurs as surrounding isotropic garnet. Therefore, it is considered that anisotropic garnet was formed later than isotropic garnet. Anhedral magnetites are contained in garnet grains as a relict mineral. It was considered to magnetite was replaced by garnet. Chlorite and calcite observed in garnet facies as alteration products of garnet. Acicular hematite and minute pyrite scattered in magnetite. Some magnetites are replaced by hematite along to grain boundaries or fractures.

Wollastonite facies is generally developed between chlorite facies and garnet facies. Wollastonite facies is composed of wollastonite, garnet and calcite, with small amounts of quartz, hematite and magnetite. Wollastonite occurs as monomineralic aggregates of fibrous or prismatic crystals. Wollastonite is partly replaced to subhedral to euhedral grossular garnet (Fig. 4B). The garnet tends to occur in polycrystalline aggregates and in areas occurs as nearly monomineralic garnet. Two types of garnet are recognized. Isotropic garnet occurs in central part of grain, which surround iron-oxides. Anisotropic garnet formed marginal part of coarser grain. The anisotropic garnet seems to be formed by recrystallization

Facies Minerals	Skarn stage			
	Garnet	Wollastonite	Epidote	Chlorite
Quartz				
Wollastonite				
Epidote				
Garnet	Ad98-Ad82	Ad95-Ad60	Ad63-Ad50	
Chlorite				
Muscovite				
Calcite				
Magnetite				
Hematite				
Scheelite				
Pyrite				
Chalcopyrite				
Pyrrhotite				
Sphalerite				
Galena				

Fig. 5. The skarn facies and paragenetic sequences of minerals.

of the isotropic one. It is difficult to distinguish the strongly anisotropic garnet in wollastonite facies and that in garnet facies. Garnet replaced by calcite in patches. Calcite occurs as vein-like in shape and fills garnet-lined vug (Fig. 4B).

Epidote-(scheelite) facies have been observed directly in contact with chlorite facies, and occurs as vein-like mass between quartz-mica schists and chlorite facies. This facies accompanied with fairly amounts of scheelite (Fig. 4C). Epidote facies consists of quartz, epidote, garnet, scheelite and minor amounts of magnetite, chlorite and calcite. Garnet is optically anisotropic and shows a zonal structure. Fine-grained garnet is included in epidote. Euhedral to subhedral scheelite occurs as disseminated grains in quartz and epidote. The grain size is generally 2 to 4 mm (up to 10 mm). Scheelite has a blue-white fluorescence in ultraviolet light. Small amounts of chlorite and calcite occur as veinlets in quartz, epidote, garnet and scheelite. Minute grains of magnetite and hematite are often included in quartz, epidote and scheelite.

Chlorite facies is developed between epidote facies and wollastonite facies. It also occurs along the contacts between garnet facies and quartz-mica schist. Calcite veins are common developed in the facies. Chlorite facies is mainly composed of chlorite, muscovite and calcite with small amount of quartz, pyrite, chalcopyrite, sphalerite, galena and hematite (Fig. 4D). Chlorite occurs

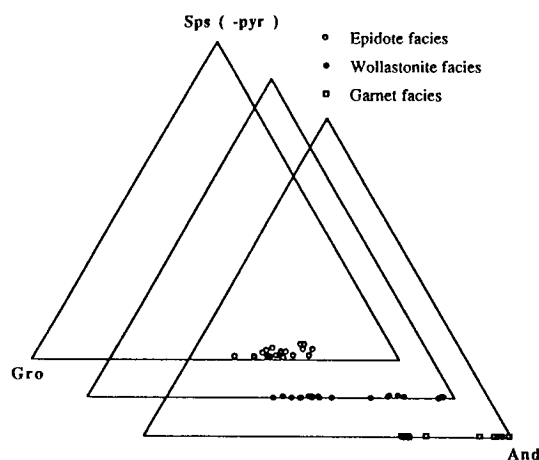


Fig. 6. Spessartine (- pyrope) - grossular - andradite diagram showing compositional variation of garnet in different skarn facies.

as radiating aggregates or discrete grains. Fan-shaped muscovite and anhedral quartz occur in interstices and inside of calcite. Subhedral to euhedral calcite is usually show hexagonal cleavages. Flaky and radial aggregates hematite is partly replace to magnetite. Sulfides are associated commonly with chlorite facies. The sulfides sometimes occurs as veinlet which contain calcite, quartz and chlorite, but do not contain calc-silicate minerals. Pyrite, in coarse euhedral to subhedral grains, frequently encloses magnetite and containing small droplike pyrrhotite inclusions is also present. Sphalerite mostly appears to have crystallized later than chalcopyrite. However, some sphalerite contains bleblike inclusions of chalcopyrite. This sphalerite is relatively iron-poor (1~5 mole% FeS). Galena fill space between calc-silicates and is commonly replaced by sphalerite. Some chlorite, epidote and sericite is formed by alteration of garnet and epidote. The mineralogical changes which occur in this paragenetic sequence of skarn facies at Chungju mine are summarized in Fig. 5, but the alteration stage is not summarized.

MINERAL COMPOSITIONS IN SKARN

The main skarn minerals, garnet, epidote, wollastonite, scheelite, chlorite, muscovite and calcite were analyzed by an electron probe microanalyzer.

Garnet occur as one of the abundant and show the wide-ranged chemical variation in dominant solid solution of grossular and andradite (Table 2). Two types of garnet are recognized in skarn. Compositional zoning

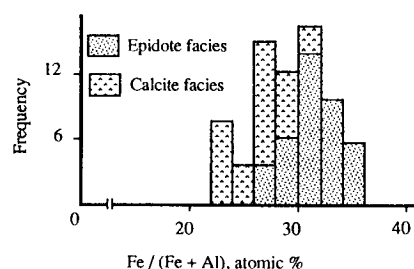


Fig. 7. $\text{Fe}^{3+}/(\text{Fe}^{3+} + \text{Al})$ ratio corresponding to pistacite molecule in epidotes.

is common. Cores are higher Fe and Mn content than rims, but Al is higher in rims than in cores. The most Ca-depleted garnets occur in epidote facies, whereas more Ca-rich garnets occur in garnet facies and wollastonite facies. The chemical compositions of garnet may be expressed almost entirely in term of the three end members in spite of negligible amounts of almandine molecule; grossular, andradite and spessartine(-pyrope) (Fig. 6). Garnet in epidote facies shows little compositional variation as function of differences in optical properties, and the andradite/(andradite + grossular) mole fraction is 0.64 to 0.73, and garnet containing epidote facies is always anisotropic.

On the other hand, the chemical composition of garnet in garnet facies and wollastonite facies can be divided into two groups on the basis of its optical properties. Anisotropic garnet shows 0.70 to 0.72 from garnet facies, and 0.60 to 0.63 from wollastonite facies in andradite/(andradite + grossular) mole fraction, and isotropic garnet shows more than 0.96 (Table 2). Garnet having an intermediate composition (0.84) is rarely observed in wollastonite facies. Garnet in epidote facies tends to increase in Fe, Mn and Ti and decrease in Al from core to rim. The garnet contains relatively high MnO_2 (up to 1.83 wt.%) and TiO_2 (0.92 wt.%). Variations in garnet compositions indicate aluminum contents becomes progressively more enriched and iron decreased toward the later stage of skarn evolution.

Epidote generally occur as an aggregate of subhedral to euhedral crystals with high birefringence in epidote facies. Epidote occurs as veinlets and also as an alteration product of garnet in chlorite facies. Epidote is well represented by the binary system, $\text{Ca}_2\text{Al}_2\text{Si}_2\text{O}_{12}(\text{OH})$ (clinozoisite) and $\text{Ca}_2\text{AlFeSi}_2\text{O}_{12}(\text{OH})$ (pistacite), and shows a significant variation in $\text{Fe}^{3+}/(\text{Fe}^{3+} + \text{Al})$ mole fractions in the M3 site of epidote. The composition of epidote are shown in Table 3. The $\text{Fe}^{3+}/(\text{Fe}^{3+} + \text{Al})$ mole fractions of epidote range from 0.25 to 0.35 (Fig. 7). Their pistacite component ($X_{\text{ps}}: \text{Fe}^{3+}/(\text{Fe}^{3+} + \text{Al})$) does not

Table 2. Microprobe analyses of garnet from different facies in Chungju mine.

Optical properties*	Garnet facies						Wollastonite facies						Epidote facies					
	I	I	I	A	A	A	I	I	I	A	A	A	I	I	I	A	A	A
SiO ₂	35.20	35.58	35.13	36.65	36.68	37.11	35.29	35.64	35.94	36.33	36.25	36.35	36.35	36.64	36.98	36.63	37.5	37.02
Al ₂ O ₃	0.68	0.71	0.56	6.03	5.92	6.14	0.8	0.84	3.31	8.69	8.45	7.85	6.6	6.75	6.13	7.17	7.73	7.36
TiO ₂	0.13	0.16	0.17	0.01	0.18	0.07	0.19	0.2	0.84	0.08	0.22	0.2	0.26	0.27	0.32	0.17	0.14	0.24
FeO ₃	31.27	30.89	31.50	23.92	23.89	23.03	30.45	30.27	27.15	20.4	20.27	20.57	25.59	24.91	25.73	22.36	21.38	21.78
MnO	0.07	0.08	0.07	0.10	0.03	0.09	-	-	0.19	0.14	0.09	0.09	1.79	1.83	0.98	0.55	0.51	0.58
MgO	0.01	-	0.01	0.01	-	-	0.06	0.03	0.01	0.02	0.02	-	0.09	0.06	0.08	0.03	0.03	0.02
CaO	32.57	33.08	32.39	33.70	33.25	33.42	33.08	33.37	33.05	34.37	34.63	34.79	29.51	29.54	30.05	33.05	32.69	32.98
Total	99.93	100.50	99.83	100.42	99.95	99.86	99.87	100.4	100.5	100	99.93	99.85	100.5	100.3	100.1	99.96	99.98	99.98
Formulas on the basis of 24(O)																		
Si	5.948	5.971	5.945	5.977	6.001	6.057	5.958	5.982	5.94	5.887	5.885	5.918	5.964	6.009	6.004	5.967	6.06	6.01
Al	0.134	0.140	0.112	1.158	1.141	1.182	0.159	0.167	0.645	1.66	1.617	1.506	1.265	1.293	1.179	1.377	1.471	1.408
Ti	0.017	0.021	0.021	0.002	0.022	0.009	0.024	0.025	0.104	0.01	0.026	0.024	0.032	0.033	0.04	0.02	0.017	0.029
Fe ³⁺	3.975	3.900	4.010	2.935	2.941	2.827	3.868	3.821	3.375	2.487	2.476	2.519	3.133	3.046	3.159	2.741	2.6	2.66
Mn	0.009	0.011	0.010	0.013	0.004	0.013	-	-	0.027	0.019	0.013	0.013	0.247	0.252	0.135	0.076	0.07	0.079
Mg	0.003	-	0.004	0.003	-	-	0.014	0.006	0.003	0.005	0.005	-	0.022	0.015	0.018	0.006	0.008	0.005
Ca	5.894	5.946	5.870	5.887	5.827	5.843	5.981	5.998	5.851	5.964	6.021	6.066	5.144	5.141	5.252	5.767	5.659	5.735
Total	15.980	15.989	15.972	15.975	15.936	15.931	16	16	15.95	16.03	16.04	16.05	15.81	15.79	15.79	15.95	15.89	15.93
Mole percent																		
Andradite	96.8	96.6	97.3	71.7	72.2	70.4	96.1	95.8	84.4	60.1	60.7	62.8	71.4	70.4	73.1	66.7	64.0	65.6
Grossular	2.9	3.2	2.4	28.0	27.7	29.2	3.7	4.1	15.0	39.5	39.0	37.0	23.6	24.7	24.1	31.9	34.7	32.9
Spessartine	0.1	0.0	0.1	0.1	0.0	0.0	0.2	0.1	0.1	0.1	0.1	0.0	0.4	0.2	0.3	0.1	0.1	0.1
Pyrope	0.2	0.2	0.2	0.2	0.1	0.4	0.0	0.0	0.5	0.3	0.2	0.2	4.6	4.7	2.5	1.3	1.2	1.4

I = Isotropic garnet, A = Anisotropic garnet

Table 4. Microprobe analyses of scheelite from Chungju mine.

Sample no.	CaO	SeO ₂	MoO ₃	WO ₃	Total
CJ-321-1	20.52	0.62	0.14	78.85	100.13
CJ-321-2	20.86	0.71	0.15	78.41	100.13
CJ-372-1	20.64	0.73	0.13	78.51	100.01
CJ-372-2	20.75	0.77	0.15	78.52	100.19
CJ-780-1	20.34	0.59	0.12	78.57	99.62
CJ-780-2	20.75	0.54	0.16	78.62	100.07

show any systematic compositional pattern within a single grain, while it tends to decrease toward the chlorite facies ranging from 0.31 down to 0.25. The Fe³⁺ content of epidote tendency to decrease systematically toward the host rock side.

Wollastonite composition is nearly pure. CaO content in the wollastonite range from 46 to 47 wt.%.

Scheelite shows pale blue to white fluorescent color under a radiation of ultraviolet light. Although the relationship between the fluorescent colors and molybdenum contents of scheelite has been found by Greenwood (1943), Kononov (1968), Shoji and Sasaki (1978), and Kim (1979), detailed electron microprobe analyses

revealed that scheelite from the Chunju mine is nearly pure CaWO₄. However, are detected in scheelite minor amounts of serium, up to 0.8 wt.%(Table 4).

Chlorites replace andraditic garnet or filled interstices of calc-silicates. Flakes shaped chlorite occur in a matrix of calcite with only traces of any calc-silicate minerals remaining. Chlorite associated with this calcite alteration has a uniformly low iron content. The lower iron chlorite are usually pale green in color. The Fe/(Fe+Mg) ratio of these chlorite is 0.60 to 0.62, which is lower than that of chlorite in the garnet facies(0.82 to 0.86)(Table. 5).

Muscovite occur as phengite of the muscovite-celadonite solid solution series(Table. 5). It contains varying amount of iron (4.02~5.57% as FeO) and magnesium (0.38~0.68% MgO).

Calcite is essentially pure CaCO₃. CaO content in calcite range from 55 to 58 wt%. Contents of FeO, MgO and MnO are often less than 1wt%. Electron microprobe analyses of the sphalerite has an iron content ranging from 1.4 to 5.5(mole% FeS).

Although the rocks are mineralogically heterogeneous, a number of distinctive types of skarn have been recognized. There are several important features of mineral composition. Isotropic garnets show extremely pure an-

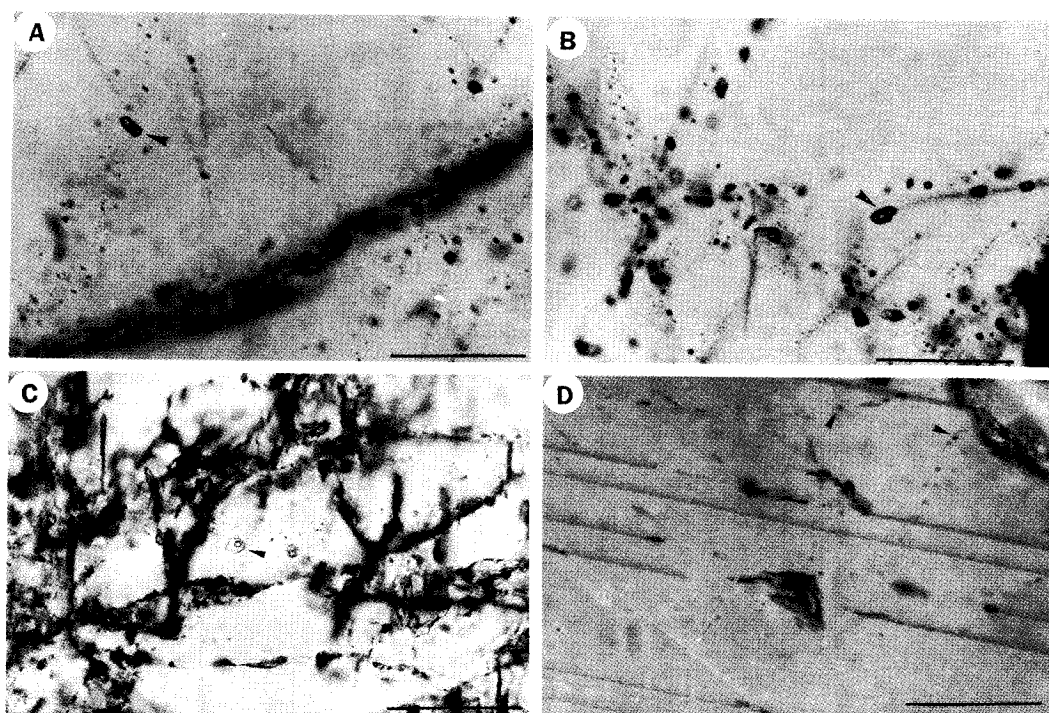


Fig. 8. Microphotographs of fluid inclusions from skarn. A; Two- phase inclusions in quartz, B; Two- phase inclusions in scheelite, C; Two- phase inclusions in epidote, D; Two- phase inclusions in later stage calcite. Scale bars indicate 0.1 mm.

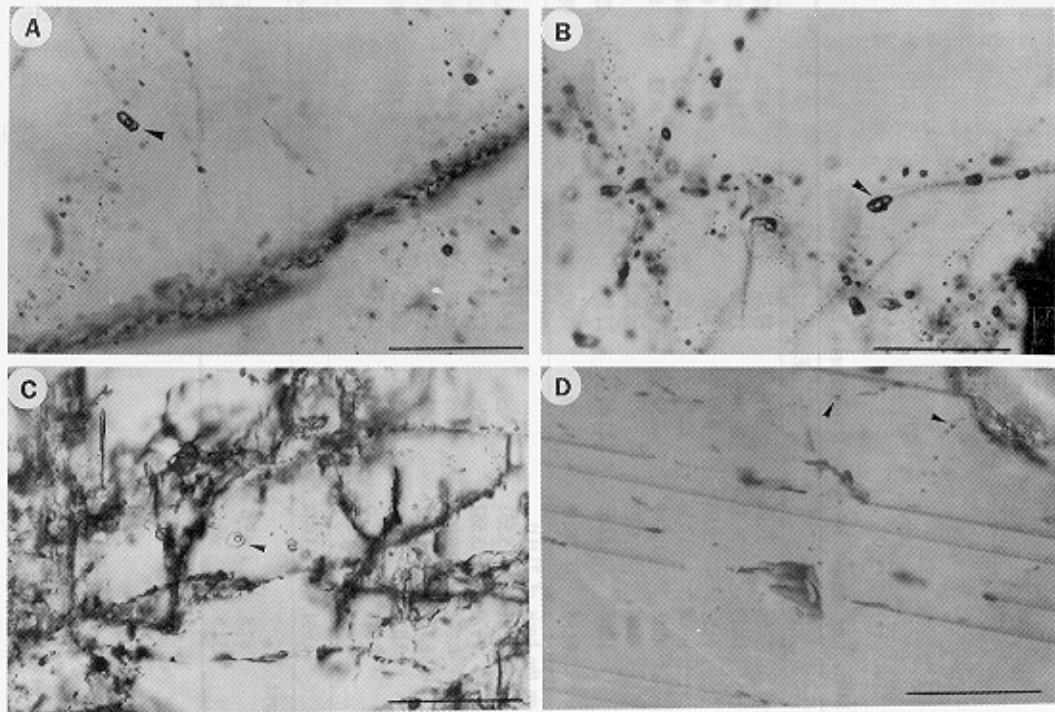


Fig. 8. Microphotographs of fluid inclusions from skarn. A; Two- phase inclusions in quartz, B; Two- phase inclusions in scheelite, C; Two- phase inclusions in epidote, D; Two- phase inclusions in later stage calcite. Scale bars indicate 0.1 mm.

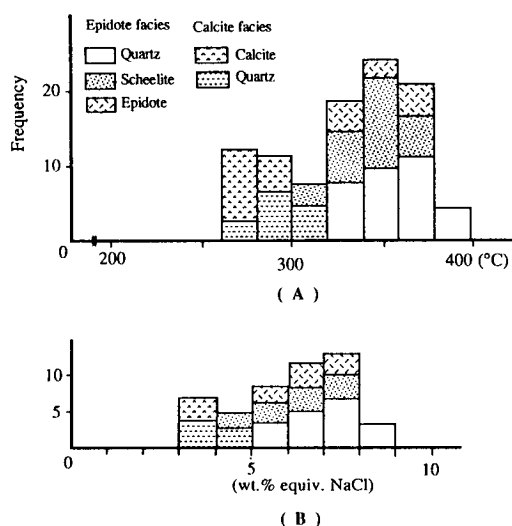


Fig. 9. Homogenization temperatures (A) and salinities (B) of fluid inclusions.

dradite(>Ad 96) in garnet facies. Anisotropic garnet in epidote facies is more aluminous (\approx Ad 60) than isotropic garnets. Epidote composition becomes lower in Fe^{3+} (pistatite mole%; from Ps35 in epidote facies to Ps25 in chlorite facies). Early magnetites which occur in garnet facies were replaced by hematite. The $\text{Fe}/(\text{Fe} + \text{Mg})$ molar ratio of chlorite varies from 0.86 to about 0.62.

FLUID INCLUSION STUDIES

Fluid inclusion measurements were made on quartz, scheelite, epidote and calcite. Fluid inclusions occur in various size and shapes, but all consist of liquid and vapor, in which the liquid phase usually makes up 60 to 80 percent of the total inclusion volume at room temperature. Fluid inclusions ranges from <1 to $30\text{ }\mu\text{m}$ in size, but usually from 5 to $10\text{ }\mu\text{m}$ in length. All measurements were made on inclusions larger than $5\text{ }\mu\text{m}$. The majority of fluid inclusions are in the garnet growth zones, suggesting a primary origin, but they were not analyzed because of their very small size ($<3\text{ }\mu\text{m}$). Most of the fluid inclusions in quartz(epidote facies) are scattered through grains and have cubic to negative crystal shape with round edge or oval shape, or occur as irregular shape, but some are concentrated within planes that appear to be growth zones or fractures(Fig. 8A). Fluid inclusions in scheelite are commonly polygonal or rectangular form with round edge and are either isolated or aligned along planes(Fig. 8B). Epidote and calcite contains fluid inclusions of isolated irregular shape(Fig.

8C, D). In all cases, only inclusions considered to be primary, according to criteria of Roedder(1979, 1984), were used for microthermometric analysis. No liquid carbon dioxide is observed on freezing. The lack of any visible liquid CO_2 suggests that the inclusions are H_2O -rich. Highly saline inclusion, with containing liquid, vapor bubble, and at least a halite daughter crystal, are not observed at the samples. All fluid inclusions analyzed were homogenized to a liquid phase without any phase change between room temperature and the homogenization temperature. The homogenization temperatures of fluid inclusions in skarn minerals have a wide range from 392°C to 258°C . Salinities of fluid inclusions range from 3.2 to 8.5 wt.% equivalent of NaCl. Results of the measurements of homogenization temperatures of fluid inclusions are summarized in Fig. 9. The homogenization temperatures of fluid inclusions of epidote facies and calcite facies have range from $320\sim 392^\circ\text{C}$ and $258\sim 312^\circ\text{C}$, respectively.

SULFUR ISOTOPE

The sulfur isotope analyses were performed on coexisting pyrite, galena collected from chlorite facies, which characterized by pyrite + chalcopryrite + sphalerite + galena assemblages. The sulfur isotopic compositions are reported in the usual $\delta^{34}\text{S}$ per mil notation relative to Canon Diablo Troilite. The reproducibility of replicate analyses of a mineral sample is usually better than ± 0.1 per mil.

The $\delta^{34}\text{S}$ values and mineral association in each sample from the skarn are listed in Table 6. It reveals both the strong uniformity and the similarity in isotopic composition of pyrite($9.51 \pm 0.04\text{‰}$), and galena($5.85 \pm 0.05\text{‰}$). In particular, there are no marked differences in $\delta^{34}\text{S}$ between pyrite and galena from the chlorite facies.

ENVIRONMENT OF SKARN FORMATION

Main prograde metasomatic process in early skarn facies have started with the formation of andradite, wollastonite and magnetite, through the formation of epidote, grossular-rich garnet, and scheelite, and ended with the formation of chlorite, muscovite, calcite and sulphides. The absence of pyroxene and the common occurrence of high content of Fe^{3+} minerals indicates that early facies generally determines an higher temperature and oxygen fugacity, and lower X_{CO_2} limit for the skarn formation. On the other hand, the late skarn facies is retrograde, in which the hydrous alteration of the pre-existing skarn minerals and formation of hydrous silicates, carbonate and sulphides are prevailed. That is,

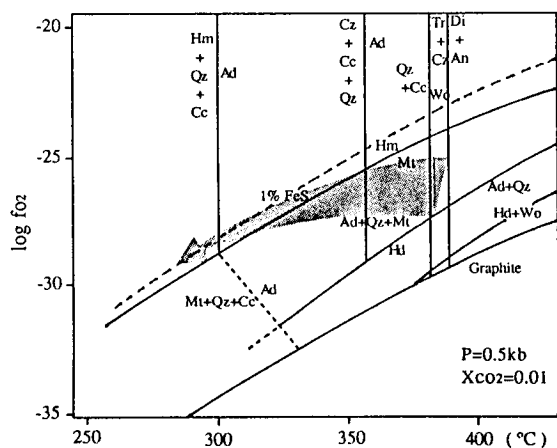


Fig. 10. Temperature-oxygen fugacity ($\log f_{O_2}$) diagram for the system $\text{CaO-FeO-Fe}_2\text{O}_3\text{-Al}_2\text{O}_3\text{-SiO}_2\text{-H}_2\text{O-CO}_2$ at $X_{\text{CO}_2} = 0.01$ and total pressure = 0.5 kb (see text). The hatched area shows the f_{O_2} condition during skarn formation. Abbreviations: Cc; calcite, Ad; andradite, Hd; hedenbergite, Hm; hematite, Mt; magnetite, Qtz; quartz, Cz; epidote, Wo; wollastonite, Di; diopside, An; anorthosite, Tr; tremolite.

garnet and wollastonite are replaced by chlorite, calcite and muscovite. The evolution of ore forming fluids has started with the formation of magnetite during the early facies, and has been immediately followed by the scheelite impregnation during the end of this early facies. The late facies has started with the formation of hematite and sulphides in lower f_{O_2} and temperature, and relatively sulfur fugacity increasing conditions than early facies. T- f_{O_2} diagram at 0.5 kb and 0.01 of X_{CO_2} showing the equilibria applicable to the skarn assemblages is represented in Fig. 10. This diagram shows only the equilibria relevant to skarn parageneses. The cross-hatched area represents the area of coexistence of garnet, wollastonite, epidote, chlorite, iron oxide, and other minerals. The thermochemical data for the minerals are from Helgeson et al. (1978). Solid line calc-silicate equilibria is based on experimental data from Liou (1974), Gustafson (1974), Taylor and Liou (1978). The f_{O_2} buffers are based on French and Eugster (1968) and French (1971). The FeS content of sphalerite (mole% FeS = 1~5%) is based on the data of Scott and Barnes (1971) and French (1971). To determine the environment of skarn formation, it is necessary to consider the effects of variable oxygen and sulfur fugacities in addition to temperature, pressure and X_{CO_2} .

The homogenization temperatures of fluid inclusions in skarn minerals have a wide range from 392°C to 258°C (Fig. 6). Stable isotope geothermometry about $283 \pm 20^\circ\text{C}$ for the pyrite-galena pairs of coexisting sulfide

minerals from chlorite facies. This temperature range is lower part may be equivalent to the temperature range obtained from homogenization temperatures of fluid inclusion. Pressure estimated from fluid inclusion is approximately 400 bars.

The stability field of the dominant skarn calc-silicate minerals, garnet, wollastonite, epidote and chlorite can be discussed as functions of oxygen fugacity and temperature at a reasonable value of X_{CO_2} . Temperatures and X_{CO_2} are poorly constrained by the andradite- and wollastonite-terminal reactions (Greenwood, 1967; Taylor and Liou, 1978). The presence of wollastonite in the early skarn facies is suggested by the reaction: $\text{CaCO}_3 + \text{SiO}_2 = \text{CaSiO}_3 + \text{CO}_2$. The common occurrence of andradite garnet apparently coexisting with its decomposition products suggest that, as temperature dropped, CO_2 fugacities were approximately buffered by the reaction: $\text{andradite} + 3\text{CO}_2 = 3\text{calcite} + \text{hematite} + 3\text{quartz}$. The absence of visible liquid CO_2 around the gas bubble in the fluid inclusions are very H_2O -rich, with a maximum X_{CO_2} of about 0.01, temperature minima are approximately 300°C and 381°C from the above reactions. Thus it would appear that a reasonable value for X_{CO_2} during skarn formation is about 0.01. Using this value for X_{CO_2} , the oxidizing-reducing capacity of skarn environment as function of temperature can be deduced. At even lower values of X_{CO_2} , the stability field of andradite would be larger. Epidote composition is considered to be highly dependent on oxygen fugacity (Holdaway, 1972; Liou, 1973). Chemical data for epidote in this deposit suggest that the mineral containing a pistacite component of up to about 35 percent is stable to magnetite-hematite buffer to lower than magnetite-hematite buffer. Clinopyroxene is not observed in the skarn assemblage, a reasonable lower f_{O_2} limit for andradite is the (andradite + quartz + magnetite)-hedenbergite buffer. The upper limit of f_{O_2} is mostly down of magnetite-hematite buffer (garnet facies) and upper of hematite-magnetite buffer (chlorite facies). The products of late alteration of garnet reflect the garnet composition. The common occurrence of andradite garnet apparently coexisting with its decomposition products suggest that, as temperature dropped, CO_2 fugacities were approximately buffered by the reaction: $\text{andradite} + 3\text{CO}_2 = 3\text{calcite} + \text{hematite} + 3\text{quartz}$. However, chlorite usually appears to be one of the alteration products of garnet, chlorite formation may be a consequence of the aluminum content of most of the garnet. This suggests a reaction: $\text{andradite-grossular} + \text{CO}_2 + \text{H}_2\text{O} = \text{calcite} + \text{hematite} + \text{quartz} + \text{chlorite}$. Chemical data for chlorite show a higher content of magnesium. The assemblages of ore minerals also indicate f_{O_2} conditions

Table 5. Microprobe analyses of chlorite and muscovite from chlorite facies in Chungju mine.

	Chlorite (O=28)								Muscovite (O=22)			
SiO ₂	26.15	25.02	23.80	22.30	26.78	26.23	25.75	26.13	46.96	46.07	47.03	46.81
Al ₂ O ₃	18.38	19.12	21.27	20.98	19.60	19.02	19.13	18.94	29.26	28.96	30.13	29.14
TiO ₂	0.05	0.06	0.00	0.04	0.03	0.03	0.07	0.05	0.08	0.19	0.07	0.11
FeO	37.04	37.92	36.78	37.36	30.09	30.11	30.64	30.01	4.40	5.57	4.02	4.96
MnO	1.04	0.96	0.57	0.74	0.10	0.12	0.23	0.25	0.03	0.01	0.04	0.02
MgO	4.62	4.22	3.77	3.36	10.45	10.38	10.45	11.12	0.68	0.38	0.52	0.57
CaO	0.03	0.04	0.23	0.67	0.02	0.02	0.04	0.01	0.03	0.03	0.02	0.02
Na ₂ O	0.01	0.05	0.27	0.08	0.06	0.00	0.06	0.03	0.19	0.27	0.22	0.23
K ₂ O	0.32	0.13	0.08	0.06	0.12	0.04	0.09	0.03	9.65	9.31	9.68	9.66
Total	87.65	87.53	86.77	85.59	87.27	85.95	86.45	86.58	91.28	90.79	91.73	91.52
Si	5.910	5.696	5.434	5.227	5.802	5.785	5.675	5.726	6.587	6.537	6.549	6.572
Al	4.895	5.132	5.724	5.796	5.005	4.943	4.971	4.891	4.837	4.842	4.944	4.821
Ti	0.009	0.011	0.000	0.007	0.005	0.004	0.012	0.008	0.009	0.020	0.007	0.012
Fe ²⁺	7.000	7.221	7.023	7.322	5.451	5.554	5.649	5.500	0.516	0.661	0.468	0.582
Mn	0.199	0.185	0.110	0.147	0.018	0.023	0.006	0.046	0.003	0.001	0.004	0.002
Mg	1.556	1.434	1.284	1.175	3.374	3.412	3.434	3.633	0.142	0.080	0.108	0.119
Ca	0.008	0.010	0.056	0.168	0.005	0.005	0.008	0.003	0.004	0.004	0.003	0.003
Na	0.006	0.021	0.118	0.036	0.026	0.000	0.024	0.013	0.051	0.073	0.059	0.063
K	0.092	0.039	0.022	0.019	0.034	0.010	0.024	0.009	1.726	1.685	1.719	1.729
Total	19.674	19.750	19.772	19.895	19.721	19.736	19.804	19.831	13.875	13.903	13.861	13.903

Table 6. Sulfur isotopic composition (per mil) for samples from chlorite facies.

Sample no.	mineral	$\delta^{34}\text{S}(\text{‰})$	$\Delta_{\text{py-gn}}$	T(°C)
CJS-1	pyrite	9.13	py1-gn1	3.28
	galena	9.51	py1-gn2	3.16
CJS-2	pyrite	5.85	py2-gn1	3.58
	galena	5.96	Average	3.34
				283 \pm 20°C

intermediate between the hedenbergite-andradite-magnetite-quartz and hematite-magnetite buffer. Therefore, it is thought that the skarns and ore minerals were formed in the hatched region(Fig. 10). The oxygen fugacity(f_{O_2}) of the skarn mineralization decreased with time. The early skarn facies would have formed at log f_{O_2} values of about -25 to -27 , and late skarn facies would have formed at log f_{O_2} values of -28 to -30 . Temperature of the skarn mineralization are estimated to be in the range of 392°C to 258°C and pressure to be 0.5 kb, and at $X_{\text{CO}_2}=0.01$.

TUNGSTEN MINERALIZATION

Scheelite which is one of the important ore minerals are mostly concentrated in the epidote facies. Field and microscopic evidences generally indicate that scheelite mineralization is slightly later than the magnetite, garnet and wollastonite, and is followed by the formation of

chlorite, hematite and sulfides. General studies have suggested that tungsten skarn deposits can be divided into two subclasses, reduced type and oxidized type (Newberry, 1982; Kwak and White, 1982) or scheelite type and molybdo-scheelite type(Sato, 1977b). Mineral assemblage and mineral composition of skarns are different between the two subclasses. Molybdenum-bearing scheelite in skarns tends to be associated with relatively oxidized mineral assemblages(Sato, 1977a, 1980). The formation of highly pure scheelite could have resulted from the reduced environment as well as from Mo-poor condition. Scheelite from the Chungju deposit is practically free from molybdenum(Table 4) and shows white-blue fluorescent color. The tungsten mineralization occurred in the epidote facies and at intermediate oxidation, and minor sulfides deposition occurred in the chlorite facies and at lower oxidation and higher sulfidation states, as expressed by the hematite-pyrite-chalcopyrite-sphalerite-galena assemblage. These features and the estimated physicochemical environment lead to a possible mechanism of skarn deposition involving a decrease in oxidation state and temperature. This observation obtained from Chungju skarn is consistent with the conclusion of Hsu and Galli(1973) and Hsu(1977), that an oxidized environment favors the formation of CaMoO_4 -rich scheelite, whereas a reduced one results in purer scheelite along with molybdenite. The homogenization temperatures of fluid inclusions in scheelite

have a range from 370°C to 310°C. Salinities of fluid inclusions in scheelite range from 4.2 to 6.5 wt.% equivalent of NaCl. There is a distinct indication that homogenization temperatures for scheelite were lower than the homogenization temperatures for quartz of early stage. Scheelite mineralization were formed by lowering in the oxygen fugacity (reduction of the ore-forming fluid) in addition to the decrease of the Ca and Fe³⁺ concentration in the associated fluid with decreasing temperature condition. The estimated physicochemical environment during skarn formation suggest that the principal causes of scheelite mineralization are a reduction of the ore-forming fluid and a decrease in temperature.

CONCLUSIONS

1) Chungju skarn were derived from the quartz-mica schist surrounding the biotite granite. Skarn mineralization are formed extensively from alumina and silica-rich quartz-mica schist by the introduction of calcium and iron from hydrothermal solution. The mineral assemblage and mineral compositions suggest that the chemical potentials of Ca and Fe increased toward the biotite granite, and the component of Al, Mg, K, and Si decreased from the host rock to biotite granite (from chlorite facies to garnet facies).

2) The skarn process in the time-evolutional trend can be divided broadly into the four facies in terms of the paragenetic sequence of calc-silicates and their chemical composition. Skarn and ore minerals were formed in the following sequence; (1) garnet facies, adjacent to biotite granite, containing mainly garnet (>Ad96) and magnetite (2) wollastonite facies containing mainly wollastonite and garnet (Ad95~60), (3) epidote facies, containing mainly epidote (Ps35~31), quartz, andradite-grossular (Ad63~50), and scheelite, (4) chlorite facies, adjacent to and replacing schist, containing mainly chlorite, muscovite, quartz, calcite, epidote (Ps31~25), hematite and sulfides.

3) Mineral assemblages and fluid inclusion data indicate that skarn were formed at low X_{CO_2} , approximately 0.01. Temperature of the skarn mineralization are estimated to be in the range of 400 to 280°C and pressure to be 0.5 kbar. Early skarn facies formed under higher oxidizing conditions compared with the late skarn facies. The oxygen fugacity (f_{O_2}) of the skarn mineralization decreased with time. The early skarn facies would have formed at log f_{O_2} values of about -25 to -27, and late skarn facies would have formed at log f_{O_2} values of -28 to -30. The estimated physicochemical condition during skarn formation suggests that the principal causes of scheelite mineralization are reduction of the ore-forming

fluid and a decrease in temperature.

ACKNOWLEDGEMENTS

We are grateful for the financial supports by the Center for Mineral Resource Research (CMR). Also, the work was supported by the Korea Science and Engineering Foundation which is greatly acknowledged.

REFERENCES

- Cluzel, D., Cadet, J. P., Kim, D. H., Hwang J. H. and Lee, B. J. (1991) Early Paleozoic geodynamic evolution of the Ogcheon belt (South Korea). Stratigraphy and tectonic setting of the Ogcheon Supergroup. In Cluzel, D. (ed.), Ph.D. thesis, The Ogcheon belt (South Korea) summary, p. 51-68.
- French, B. M. (1971) Stability relations of siderite (FeCO₃) in the system Fe-C-O. *Am. Jour. Sci.*, v. 271, p. 37-78.
- French, B. M. and Eugster, H. P. (1965) Experimental control of oxygen fugacities by graphite-gas equilibria. *Jour. Geophys. Research*, v. 70, p. 1529-1539.
- Greenwood, H. J. (1967) Wollastonite: Stability in H₂O-CO₂ mixtures and occurrence in a contact metamorphic aureole near Salmo, British Columbia, Canada. *Am. Mineralogist*, v. 52, p. 1669-1688.
- Greenwood, R. (1943) Effect of chemical impurities on scheelite fluorescence. *Econ. Geol.*, v. 38, p. 56-64.
- Gustafson, W. I. (1974) The stability of andradite, hedenbergite, and related minerals in the system Ca-Fe-Si-O-H. *Jour. Petrology*, v. 15, p. 455-496.
- Helgeson, H. C., Delany, J. M., Nesbitt, H. W., and Bird, D. K. (1978) Summary and critique of the thermodynamic properties of rock-forming minerals. *Am. Jour. Sci.*, v. 278, p. 1-229.
- Holdaway, M. J. (1972) Thermal stability of Al-Fe epidote as a function of f_{O_2} and Fe content. *Contr. Mineralogy Petrology*, v. 37, p. 307-340.
- Hsu, L. C. (1977) Effects of oxygen and sulfur fugacities on the scheelite-tungstenite and powellite-molybdenite stability relation. *Econ. Geol.*, v. 72, p. 664-670.
- Hsu, L. C. and Galli, P. E. (1973) Origin of the scheelite-powellite series of minerals. *Econ. Geol.*, v. 68, p. 681-696.
- Kim, G. S. (1991) Iron mineralization in the Chungju mining district, Korea. Ph.D. Thesis, Tsukuba Univ. 102p.
- Kim, H. S. (1977) Mineralogy and petrology of the Precambrian iron deposits, Korea. *Jour. Geol. Soc. Korea*, v. 13, p. 191-211.
- Kim, K. W. and Lee, H. K. (1965) Explanatory text of the geologic map of Chungju sheet. Geological Survey of Korea. 35p.
- Kim, S. Y. (1979) Some aspects of tungsten mineralogy and geochemistry. *J. Korean Inst. Min. Geol.*, 12, p. 127-146.
- Kononov, A. V. (1968) Photoluminescent characteristics of Mo-bearing scheelite. *Acad. Sci. USSR Dokl. Earth Sci.*, 175, p. 120-123.
- Kwak, T. A. P. and White, A. J. R. (1982) Contrasting W-Mo-Cu and W-Sn-F skarn types and related granitoids. *Mining Geol.*, v. 33, p. 339-351.

- Lee, C. H. (1986) Stratigraphy and depositional environments in the Ogcheon Supergroup with the special consideration on the carbonate key beds. Dr. thesis, Univ. Tsukuba, Ibaraki, Japan.
- Lee, S. H. (1977) Genesis of the Chungju iron mine, Chungcheong-bug-do, Korea. Jour. Geol. Soc. Korea, v. 13, p. 219-236.
- Lee, S. H. (1980) Ore petrological studies on the genesis of the metamorphic iron deposits in Southern Korea. Part 3. Genesis. Jour. Geol. Soc. Korea, v. 16, p. 61-71.
- Liou, J. G. (1973) Synthesis and stability relations of epidote $\text{Ca}_2\text{Al}_2\text{FeSi}_2\text{O}_{12}(\text{OH})$. Jour. Geol., v. 14, p. 381-413.
- Liou, J. G. (1974) Stability relations of andradite-quartz in the system Ca-Fe-Si-O-H . Amer. Mineral., v. 59, p. 1016-1025.
- Newberry, R. J. (1982) Tungsten-bearing skarns of the Sierra Nevada. I. The Pine Creek mine, California. Econ. Geol., v. 77, p. 823-844.
- Ohmoto, H. and Rye, R. O. (1979) Isotopes of sulfur and carbon. In Barnes, H. L. (ed.), Geochemistry of hydrothermal ore deposits. Wiley and Sons, New York, p. 509-567.
- Reedman, A. J., Fletcher, C. J. N., Evans, R. B., Workman, D. R., Yoon, K. S., Rhyu, H. S., Jeong, S. H. and Park, J. N. (1973) The geological, geophysical and investigations in the Hwangganri area, Chungcheong-bug-do. In Report of Geological and Mineral Exploration. Part II. Report of Mineral Exploration. Geol. Min. Inst. Korea. v. 1, p. 1-118.
- Roedder, E. (1979) Fluid inclusions as samples of ore fluids. In Barnes, H. L. ed., Geochemistry of hydrothermal ore deposits, 2nd ed., p. 684-737.
- Roedder, E. (1984) Fluid inclusions. Rev. Mineral. 12, 644p.
- Sato, K. (1977a) Wolframite from the contact-metasomatic scheelite deposits of the Kiwada, Fujigatami and Kuga mines, Yamaguchi Prefecture, Japan. Mining Geol., v. 27, p. 31-37. (in Japanese with English abstract)
- Sato, K. (1977b) Two types of tungsten skarn deposits (abs.). Japanese Assoc. Min. Pet. Econ. Geol. Jour., v. 72, p. 133-134. (in Japanese)
- Sato, K. (1980) Tungsten skarn deposits of the Fujigatami mine, Southwest Japan. Econ. Geol., v. 75, p. 1066-1082.
- Shoji, T. and Sasaki, N. (1978) Fluorescent color and X-ray powder data of synthesized scheelite-powellite series as guides to determine its composition. Mining Geol., 28, p. 397-404.
- Scott, S. D. and Barnes, H. L. (1971) Sphalerite geothermometry and geobarometry. Econ. Geol., v. 66, p. 653-669.
- Taylor, B. E. and Liou, J. G. (1978) The low-temperature stability of andradite in C-H-O fluids. Am. Mineralogist, v. 63, p. 378-393.

Manuscript received 8 March 1995

충주광산 지역 계명산층의 텅스텐 스카른화작용

김근수 · 박맹언

요 약 : 충주 광산 지역은 계명산층과 이를 관입한 중생대 화강암질 암석으로 구성되며, 이들 화강암질 암석중 백악기초(134 Ma) 혹은 호준모 화강암과 계명산층을 구성하는 석영-운모 편암의 접촉부에서 회중석을 수반하는 스카른 광상이 산출된다. 스카른은 구성광물의 공생 특성과 주 구성광물의 양적인 비에 의해 석류석 스카른대, 규회석 스카른대, 녹염석 스카른대 및 녹니석 스카른대로 분류된다. 석류석의 화학조성은 초기 순수한 안드라다이트 (> Ad96)에서 후기 알루미늄 함량비가 증가하는 안드라다이트-그라슈라(Ad~50)로 점이적인 변화를 나타내며, 녹염석은 Fe^{3+} 의 함량비가 높은 고용체 상($\text{Ps}=35$)에서 알루미늄 함량비가 높은 고용체 상($\text{Ps}=25$)으로 변화하는 양상을 띈다. 광물 공생 및 화학 조성상의 특징으로 볼 때 스카른화 작용은 Ca와 Fe의 활동도가 혹은 호준모 화강암의 접촉부에서 높고 Al, Mg, K 및 Si 활동도는 석영-운모 편암내에 발달되는 스카른에서 증가하는 경향을 나타낸다. 녹염석 스카른대에서 산출되는 회중석의 유체포유물 균질화 온도는 $300\sim 380^\circ\text{C}$ 이며 NaCl 상당 염농도는 3~8wt.%로, 석영 및 녹염석 유체포유물 균질화 온도는 $320\sim 400^\circ\text{C}$ 이다. 후기 녹니석 스카른대에서 수반되는 황화광물의 황 동위원소비는($\delta^{34}\text{S}$) 황철석 9.13~9.51%, 방연석 5.85~5.96%이며, 공존하는 황철석-방연석 광물쌍에 의한 동위 원소 지질온도는 $283 \pm 20^\circ\text{C}$ 이다. 이산화탄소-물분열(XCO_2)은 L-CO_2 가 관찰되지 않으며 H_2O 가 풍부한 유체포유물로 구성되어 있는점과, 안드라다이트 및 규회석의 광물공생 특성과 대비하여 볼때 약 0.01로 추정된다. 광물공생 및 화학조성, 상 안정 관계, 유체포유물 연구, 동위원소 지질온도계 등의 연구 결과에 의해 충주광산 지역 스카른화 작용은 $400\sim 260^\circ\text{C}$ 온도 조건과 산소분압이 감소($f_{\text{O}_2} = 10^{-30} \sim 10^{-25}$)하는 환경에서 진행되었으며, 텅스텐 광화작용은 이러한 스카른 형성 과정 중 온도의 감소(350°C)와 산소분압이 감소($f_{\text{O}_2} = 10^{-27}$) 하는 조건에서 수반되었다.